
Article:
Barker, R orcid.org/0000-0002-5106-6929, Pickles, B, Hughes, TL et al. (2 more authors) (2020) Effect of transition rate and propargyl alcohol concentration on the corrosion of carbon steel during transitions in fluid composition from inhibited hydrochloric acid to sodium chloride brine. Electrochimica Acta, 338. 135877. ISSN 0013-4686

https://doi.org/10.1016/j.electacta.2020.135877

Effect of transition rate and propargyl alcohol concentration on the corrosion of carbon steel during transitions in fluid composition from inhibited hydrochloric acid to sodium chloride brine

Richard Barker[a*], Benjamin Pickles[a], Trevor L Hughes[b], Evgeny Barmatov[b] and Anne Neville[a]

[a]Institute of Functional Surfaces, School of Mechanical Engineering, University of Leeds, Leeds, LS2 9JT, UK

[b]Schlumberger Cambridge Research, High Cross, Madingley Road, Cambridge, CB3 OEL, UK

*Corresponding Author R.J.Barker@leeds.ac.uk

Abstract

A newly developed flow cell technique is used to determine the progressive corrosion rate behaviour of carbon steel during concomitant changes in HCl and propargyl alcohol inhibitor over time, analogous to that experienced during matrix acid flowback. The corrosion response was found to be largely independent of fluid transition rate. Increasing initial inhibitor concentration supressed the overall corrosion rate with two peaks in corrosion rate being observed during every dilution process; the first peak relates to a critical propargyl alcohol concentration and the second to a critical HCl molarity. Such behaviour is discussed in the context of polymeric film formation/inhibition mechanisms.

Keywords: Acidising, Carbon Steel, Acid Corrosion, Acid Inhibition, Propargyl Alcohol

1. Introduction

A recent publication [1] described a new flow cell technique and associated methods to investigate the progressive corrosion behaviour of a metal surface initially exposed to inhibited hydrochloric acid (HCl) and subsequently to a controlled fluid transition to uninhibited sodium chloride (NaCl) brine. As described in our first paper [1], the application of this work is to improve our understanding of corrosion during flowback operations after matrix acidizing treatments in oil and gas wells. This paper presents a systematic study to evaluate the effects of inhibitor (propargyl alcohol) concentration and flow rate on the corrosion behaviour of carbon steel exposed to changes in fluid chemistry from inhibited 4 M HCl to uninhibited 4 M sodium chloride brine.

A critical issue in designing the flow cell apparatus and associated methods was to select an appropriate electrochemical technique with which to monitor the progressive corrosion behaviour during the fluid transition period (typically 24 hours). We selected linear polarisation resistance (LPR) measurements, taken every 15 minutes, because they are rapid and involve very small changes in the potential relative to the open circuit potential. These features are important when the objective is to evaluate changes in corrosion rate during long periods of sample exposure. Both dilution experiments within the flow cell and static mass loss tests at fixed inhibitor and acid concentrations are used to understand the performance of PA when the inhibitor and acid concentration are changed simultaneously as a function of time. These studies were used to model different stages of acid flowback and to evaluate the factors controlling metal corrosion in a complex and dynamic environment.

Matrix acidizing is a reservoir stimulation process whereby acid is injected into sandstone or carbonate formations to improve their permeability and thereby improve the rate of hydrocarbon production. The process works predominantly by dissolving fines near the wellbore and/or by creating dissolution channels within target formations. The rapid and extensive development of matrix acidizing technology has witnessed the introduction of various additives that control acid characteristics to optimise the rate of hydrocarbon production whilst ensuring effective protection of all metallic equipment exposed to the acid during injection.

Different acid formulations are applied depending on the mineralogy and reactivity of the formation. Typically, matrix acid formulations are based on hydrochloric acid, acetic acid, formic acid or mixtures of hydrochloric and hydrofluoric acid [2]. The acid is chosen on the basis of its ability to react with and penetrate the target rock, to dissolve the appropriate minerals to produce soluble products, and it is essential that the acid contains effective corrosion inhibitors to minimise the corrosion of all metallic components exposed during acid injection [3-5].

Acid corrosion inhibitors are mixtures of organic molecules capable of adsorbing on the various steels encountered during acid injection. One particularly useful class of organic inhibitors are the polymerizable inhibitors, which include various acetylenic

alcohols. For example, propargyl alcohol (PA or CH≡C-CH_2-OH) has been widely used [6, 7]. The inhibition mechanism of polymerisable acetylenic compounds has been discussed extensively for more than 50 years. In general, the process involves inhibitor adsorption (chemi-sorption) followed by surface-catalysed polymerisation, which is supported by the low pH of the acid [8].

In addition to maximising corrosion inhibition efficiency during acid injection, it is important to minimise corrosion *after* a matrix acidizing treatment when production is restarted and unreacted acid, followed by formation fluids, travels back into the well and through the production tubing. This stage of the stimulation process is termed acid flowback. The degree of neutralisation of the injected acid in the reservoir (i.e., the acidity of the initial flowback fluid) is influenced by several factors including (i) the initial composition of the reacting acid, (ii) the composition/heterogeneity of the treated rock, and (iii) the treatment procedure, i.e. the volume of fluid injected and the shut-in time, etc. In specific circumstances, regions near the wellbore can contain unspent acid, which is able to flow back into the well and through equipment when production is restarted. Previous publications have indicated that flowback fluids can have pH values in the range of 0-3 [9-11], whilst others are fully neutralised [12]. Consequently, it is important to understand the initial corrosivity of the flowback fluid and how this transitions over time as it is diluted by the formation brine.

Conventional industry-standard test methods used to determine and optimise the performance of acid corrosion inhibitors focus on mass loss measurements and on formulations that simulate acid injection conditions [13]. Typically, glass bead blasted test coupons are immersed in the injected acid formulation for periods matched to the acid pump time (3-12 h) under isothermal conditions matched to the reservoir temperature [7, 14-17]. These mass loss tests are usually performed in a static environment, and the volume of acid per unit surface area of the test coupon is standardised to a value matching the volume/area (V/A) ratio during acid flow through the pipe used in the operation [18, 19]. For example, a V/A ratio of 21 ml in^{-2} (3.4 ml cm^{-2}) would simulate acidizing through a 5.5 inch internal diameter pipe. The V/A ratio can affect the mass loss results. Firstly, the availability of oxygen may depend on the acid volume used in the test. Secondly, if the corrosion rate is high and/or the V/A ratio is too low, the concentration of acid may decrease during the test. In such cases, acid consumption may lead to a lower cumulative mass loss relative to the case where the acid concentration is maintained throughout the exposure period. Such industry-standard test methods are not easily adapted to an evaluation of corrosion during acid flowback wherein there are transitions in fluid chemistry (acid and inhibitor concentrations) with time. This aspect has been discussed in detail in our previous publication [1].

Our first paper outlined the development of a customised flow cell and an experimental setup to more closely model the acidizing flowback process. The flow cell can be used to measure the evolution of corrosion rate during a controlled transition in fluid chemistry. The flow cell was tested and compared against a series

of static 3 h mass loss experiments matched to various points in the fluid transition. It was demonstrated that the flow cell provides reliable and reproducible results in a much shorter time and with significantly lesser volumes of acid than required for batch experiments.

2. Experimental Procedure

2.1 Materials

HS80™ (Tenaris) steel was used for all electrochemistry and mass loss tests experiments. This material is a low carbon grade steel used to fabricate coiled tubing strings. It has a ferrite/pearlite microstructure, and its elemental composition is: 0.1–0.15 wt.% C, 0.6–0.9 wt.% Mn, <0.03 wt.% P, <0.005 wt.% S, 0.3–0.5 wt.% Si, 0.45–0.7 Cr, <0.4 Cu, and <0.25 wt.% Ni. Analytical reagent grade NaCl, 4 M HCl, and PA were obtained from the supplier Sigma-Aldrich.

2.2 Static experiments methodology

2.2.1 Solution preparation and static mass loss test methodology

Initial static mass loss tests were performed using the methodology described in our previous study [1]. This methodology involved placing two wet ground specimens (surface roughness of <0.15 µm) for electrochemistry, each with an exposed surface area of 1 cm^2, into to a 1 L test solution (agitated using a magnetic stirrer) together with one larger pre-weighed specimen for mass loss measurement (area of 29±3 cm^2 and mass determined using a precision balance with an accuracy of ±0.01 mg) to maintain a V/A ratio comparable to previous experiments [1].

In every static experiment, the specimens were placed in the glass vessel (sealed and fitted with a condenser) containing 1 L of a solution with a specific fixed acid and inhibitor concentration at 80°C (achieved using a hotplate). Tests were conducted in HCl solutions which varied in concentration in order to model different stages during acid flowback. These solutions were prepared by combining 4 M HCl (with or without PA) at an appropriate ratio with 4 M NaCl brine. Experiments were conducted for 3 h, after which, the mass loss specimen was removed and rinsed with distilled water followed by acetone. Following this, residual inhibitor was removed by scrubbing with a combination of soap and water. Finally, specimens were rinsed again with distilled water, followed by acetone, before drying and re-weighing. The determined mass loss was converted to an average corrosion rate (in g m^{-2} h^{-1}) using accurate measurements of the dimensions (and surface area) of the sample prior to the experiment commencing.

The HCl concentrations evaluated in this study are shown in Table 1. The corrosion rates of HS80™ were determined in the absence and presence of PA inhibitor using the mass loss technique. The volume of PA added to each inhibited system was proportional to the concentration of acid in the system for all experiments. For example, 0.05 wt.% PA was present in the 4 M HCl solution, and 0.025 wt.% PA was

present in the solution obtained by mixing equal volumes of the 4 M HCl and 4 M NaCl solutions. This was done to model different stages during acid flowback wherein the unspent acid (containing inhibitor) is increasingly diluted with the formation brine as flowback proceeds.

Only three components were considered in this model flowback system: the steel, HCl and PA. In the oilfield application, the acidizing fluid may contain a mixture of acids, dosed with two or more organic inhibitors, optionally with an adsorption intensifier, solvent(s), and various other additives used to facilitate pumping downhole. These additives may include demulsifiers, wetting agents and iron and silicate stabilisers to reduce shale swelling [20]. Additionally, the real displacing formation brine would contain a complex mixture of inorganic ions and organic species together with soluble products of the reaction of the acid with the formation.

HCl concentration (M) in HCl–NaCl solution	**PA concentration (wt.%) in HCl-NaCl solution**	**PA (µL) used to maintain 0.05 wt.% per litre of 4 M HCl**
4 (100%)*	$5x10^{-2}$	540
2 (50%)	$2.5x10^{-2}$	270
0.6 (15%)	$7.5x10^{-3}$	81
0.4 (10%)	$5x10^{-3}$	54
0.2 (5%)	$2.5x10^{-3}$	27
0.04 (1%)	$5x10^{-4}$	5.4
$4x10^{-3}$ (0.1%)	$5x10^{-5}$	0.54
$4x10^{-4}$ (0.01%)	$5x10^{-6}$	0.054

* Percent of original 4 M acid concentration is shown in parentheses.

Table 1: Acid and PA concentrations in HCl–NaCl test solutions used in static electrochemical and static mass loss tests. All the HCl–NaCl test solutions contain 4 M chloride

2.2.2 Static electrochemistry test methodology

Details regarding the preparation of the working electrodes, the configuration of the three-electrode cell and acquisition of electrochemical data within the static system were described in our previous publication [1]. A Ag/AgCl reference electrode containing 4 M KCl (~0.197 V vs normal hydrogen electrode at 25°C) and a platinum counter electrode (area of ~0.8 cm^2) were used in conjunction with a carbon steel working electrode, creating a conventional three-electrode cell. After immersion in the test solution, the open circuit potential (OCP) of the working electrode was monitored using a multichannel ivium potentiostat and allowed to reach a stable value (typically 5 min), after which linear polarisation resistance (LPR)

measurements were started and repeated every 15 min for the entire duration of the 3 h test. The LPR measurements consisted of polarisaing the working electrode ±10 mV from the OCP at a scan rate of 0.25 mV s^{-1} every 15 minutes. OCP measurements were also recorded during these tests.

In all experiments, the resistance of the solution, R_s (ohm cm^2) was measured after LPR measurements through the implementation of electrochemical impedance spectroscopy (EIS). The value of R_s was subtracted from R_p to correct for solution resistance, and this value was ultimately used to calculate the corrosion rate transient response. In addition, in every static experiment, potentiodynamic polarisation measurements were conducted on each specimen upon completion of the 3 h test to determine Tafel constants associated with the anodic and cathodic reactions (β_a and β_c, respectively, in mV $decade^{-1}$). Anodic and cathodic Tafel polarisation plots were generated by polarising from the OCP to either +100 or –200 mV vs. OCP at a scan rate of 0.5 mV s^{-1}; the cathodic sweep was performed first, before switching to the second electrochemical specimen to generate the anodic Tafel plot. The Tafel slope measurements were then used in Eq. (1) to determine the Stern-Geary coefficient:

$$B = \frac{\beta_a \beta_c}{2.303(\beta_c - \beta_a)} \tag{1}$$

For each static system, the corrosion rate (expressed as a current density), i_{corr} (mA cm^{-2}), was calculated using the appropriate value of B and R_p:

$$i_{\mathrm{corr}} = \frac{B}{R_{\mathrm{p}}} \tag{2}$$

Thus, the corrosion rate as a function of time was obtained for each static system (12 measurements were made during the 3 h test period). Average values of corrosion rate or the reciprocal of R_p are provided in this paper together with error bars depicting the maximum and minimum measurements across multiple repeat specimens.

2.3 Once-through flow cell test methodology

2.3.1 Cell design and complete setup

The custom flow cell utilised in this study is shown in Fig. 1. The cell design enables a fresh mixture of acid/inhibitor to flow through the cell in a “once-through” process. The acid mixture entering the cell is progressively diluted over time to mimic the acid flowback process in a single experiment. The development and optimisation of the flow cell is the subject of our first paper [1].

Using the three-electrode setup integrated into the flow cell, real-time *in situ* measurements can be performed to determine changes in corrosion rate during the transition from 4 M HCl (containing inhibitor) to 4 M NaCl (without inhibitor). The carbon steel sample shown in Fig. 1 is flush mounted into the base of the cell. Electrochemical connection to the steel sample is created by soldering a wire to the reverse side of the specimen. The platinum counter electrode and Ag/AgCl reference electrode were both flush mounted into the top of the cell.

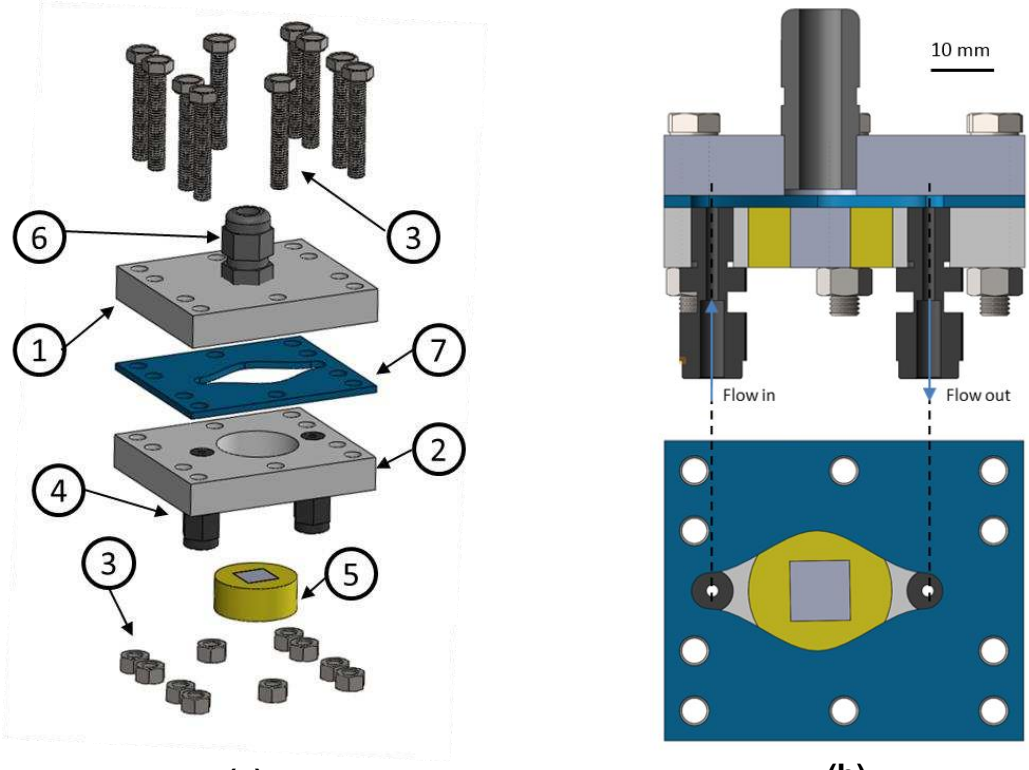

(a) **(b)**

Figure 1: (a) Exploded and (b) cross-section view of the designed flow cell. The flow cell consists of (1) a top section, (2) a base (both manufactured from an acid resistant polymer), (3) M6 bolts, (4) inlet and outlet ports, (5) a carbon steel sample sealed into the cell using non-conducting resin, (6) a cable gland to position the Ag/AgCl reference and counter into the cell, (7) a custom cut gasket manufactured from Viton™ FKM.

Fig. 2 is a schematic representation of the experimental setup within which the flow cell is integrated. The initial fluids are 1 L of 4 M HCl containing 0.01, 0.05 or 0.25 wt.% PA (depending on the experiment) and 10 L of 4 M NaCl solution. An ISMATEC® REGLO peristaltic pump was used for precise flow control (between 5 and 15 ml min^{-1} with a pump accuracy of ±5%) of NaCl solution from the 10 L container into the 1 L vessel (with the solution agitated using a magnetic stirrer). This generated a gradual decrease in the acid concentration as a function of time in the small vessel. At the same time, an identical peristaltic pump was used to transfer the solution from the 1 L vessel through a water bath to control temperature before entering the flow cell at an identical flow rate. The full setup ensured progressive dilution of the acid/inhibitor mixture with 4 M NaCl in a controlled manner.

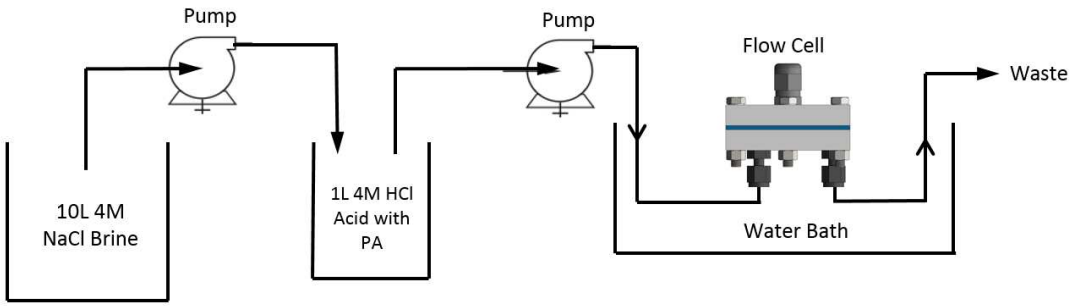

Figure 2: Schematic of experimental setup. 4 M NaCl solution is delivered at a flow rate of 5, 10 or 15 ml min^{-1} from the 10 L container into the vessel containing 1 L of 4 M HCl and 0.01, 0.05 or 0.25 wt.% PA. At the same time, the solution from the 1 L vessel is transferred (at an identical flow rate) through the flow cell and into a waste container.

2.3.2 Control of dilution rates

The rate of dilution of the 4 M HCl solution can be controlled by varying the flow rate delivered by the two peristaltic pumps. The change in the molarity of H^+ in the solution travelling through the flow cell varies as a function of the flow rate (Fig. 3) according to the general dilution equation for a constant fluid volume system [21]:

$$[H^+](t) = [H^+]_0 e^{-\frac{Qt}{V}} \quad (3)$$

where the acid molarity at a given time ($[H^+](t)$) in M is calculated from the initial acid molarity $[H^+]_0$ in M, the volume of the acid within the second vessel (V) in L, the time (t) in seconds and the volumetric flow rate (Q) in L s^{-1}. This equation is based on the assumption of a significantly smaller H^+ molarity of the diluting fluid compared to that of the fluid being diluted. In addition, the assumption of perfect mixing is also required in relation to the second vessel.

For this study, flow rates of 5, 10 and 15 ml min^{-1} (1 ml min^{-1} is equivalent to 1.66×10^{-8} m^3/s) were used to generate the different acid dilution profiles shown in Fig. 3. These dilution rates required periodic refilling of the 4 M NaCl solution within the 10 L container during the experiment.

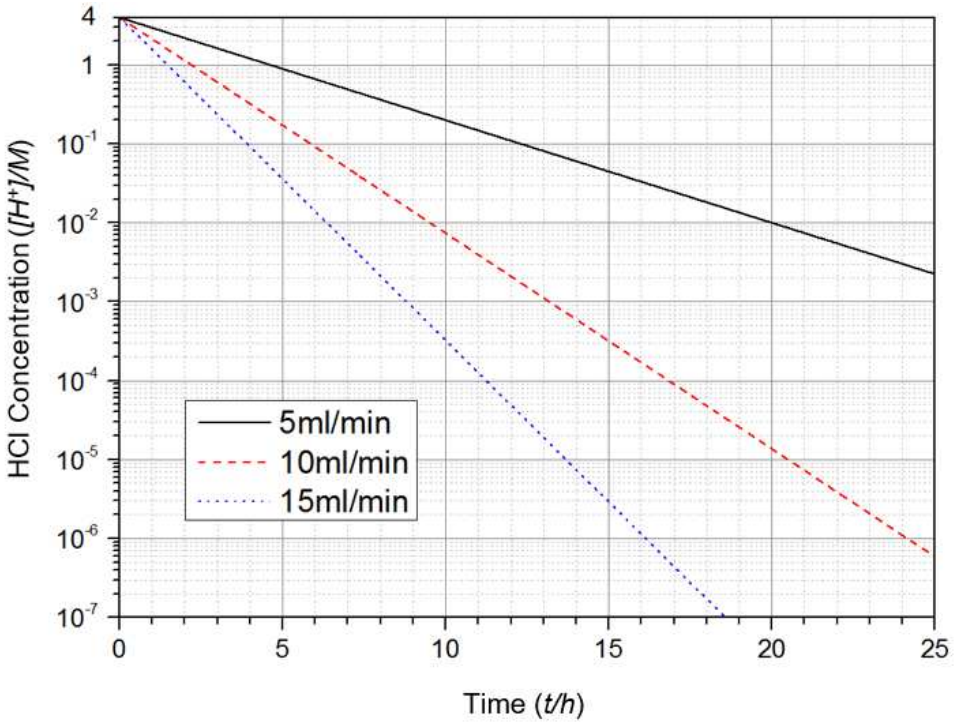

Figure 3: HCl concentration (logarithmic scale) within the flow cell as a function of time for three different flow rates. The lines representing each flow rate were derived using Eq. (3).

2.3.3 Flow cell electrochemical measurements

As regards flow cell measurements using electrochemistry, LPR measurements were also performed using the same three-electrode setup and procedure as previously outlined for static experiments.

With the exception of the first experiment (performed at 10 ml min^{-1} and initial PA concentration of 0.05 wt.%), only the reciprocal of R_p as a function of time was considered from the flow cell. This was due to the potential for variability of the Tafel constants during the dilution process. The average reciprocal of R_p from the static experiments was compared with the reciprocal of R_p measured during the progressive stages of the flow cell dilution experiment.

For the dilution experiment at 10 ml min^{-1} with 0.05 wt.% PA, an average Stern-Geary coefficient (as determined from the extensive set of static experiments) was applied to the entire fluid transition response. This enabled conversion of the measured resistances into real-time corrosion rates using Eqs. (1) and (2).

In the context of the flow cell measurements, the application of an average Stern-Geary coefficient to determine *in situ* current densities over the entire dilution profile possesses inherent limitations. That being said, such values have been provided to enable easy comparison and translation across each experiment, as well as illustrating the approximate magnitude of the corrosion rates observed, which assists

in the interpretation of the PA inhibition mechanism. In addition, the reciprocal of R_p is provided in this study, as this provides an accurate representation of the polarisation response of the specimens.

2.3.4 Flow cell experimental conditions

All experiments were performed at 80ºC. The first set of experiments evaluated the effect of dilution rate on the transient corrosion behaviour of the low carbon steel during acid (and PA) dilution. The flow rate through the cell was varied at 5, 10 and 15 ml min^{-1}, and the initial acid and PA inhibitor concentrations were fixed at 4 M and 0.05 wt.%, respectively.

In the second series of experiments, the progressive corrosion behaviour was evaluated for different initial concentrations of PA concentration (whilst maintaining the initial 4 M HCl concentration) and a flow rate of 10 ml min^{-1}. Initial PA concentrations of 0.01, 0.05 and 0.25 wt.% were evaluated.

3. Results and discussion

3.1 Corrosion rate in uninhibited HCl–NaCl solutions under static conditions

Fig. 4(a) shows average corrosion rates given by static mass loss experiments (3 h exposure, 80°C) in the absence and presence of PA at eight different initial acid concentrations ranging from 0.0004 to 4 M. In the absence of inhibitor, the corrosion rate increases from 1.4 to 685.6 g m^{-2} h^{-1} as the initial HCl concentration increases from 0.0004 to 4 M. A log-log plot of the uninhibited corrosion rate versus HCl molarity indicates a linear relationship (R^2 = 0.990) described by the equation

$$V_c = 276.9[H^+]^{0.637} \qquad (0.0004 \leq [H^+] \leq 4) \tag{4}$$

where V_c is the corrosion rate in g m^{-2} h^{-1} and $[H^+]$ is the molar concentration of protons. By comparison, Mathur and Vasudevan [22] reported that the corrosion rate of iron varied with acid concentration (HCl-H_2O solutions) according to the equation

$$V_c = ke^{B[H^+]} \tag{5}$$

where V_c is corrosion rate, k is the reaction rate constant, $[H^+]$ is acid concentration and B is an additional constant for the reaction studies. Khadom et al. [23] reported agreement with both the conventional equation of kinetics ($V_c = k[H^+]^n$) and the modified version proposed by Mathur and Vasudevan [22]. Whilst Eq. (5) matches the conventional equation of kinetics, the exponent is below 1 whereas the exponents reported by Khadom et al. [23] were between 1.144 and 1.521 for the HCl molarity range 1–5 M and temperature range 30–60˚C. Such differences in the exponent could be attributed to differences in the HCl molarity range and temperature. The results presented in Fig. 4 are determined using a broad HCl molarity range 0.0004–4 M at 80ºC in HCl-H_2O-NaCl systems with a constant chloride molarity of 4 M. Thus, the only variable in the data for the present study is

the molarity of protons, [H^+], whereas the referenced papers describe HCl-H_2O systems in which both the concentrations of H^+ and Cl^- increase with HCl concentration.

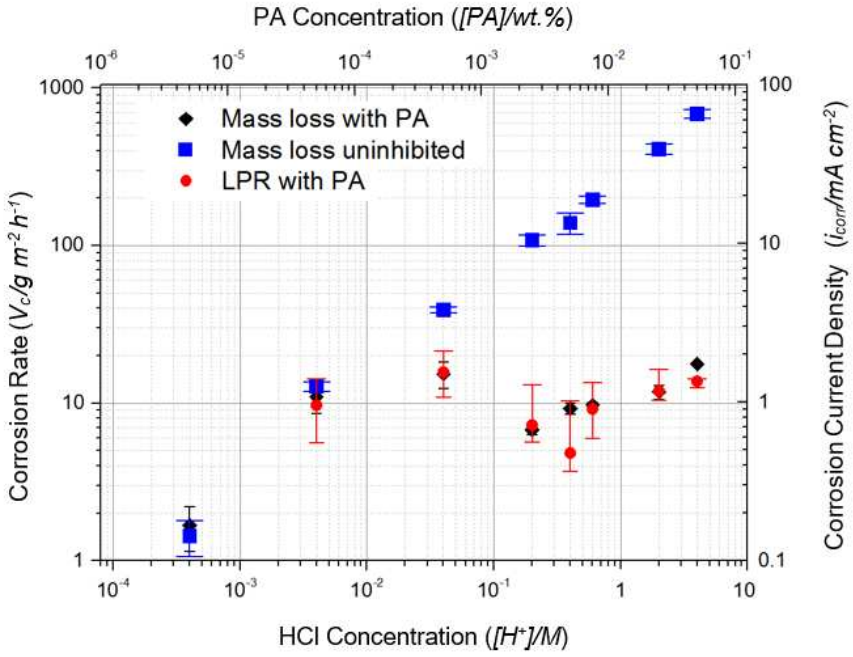

(a)

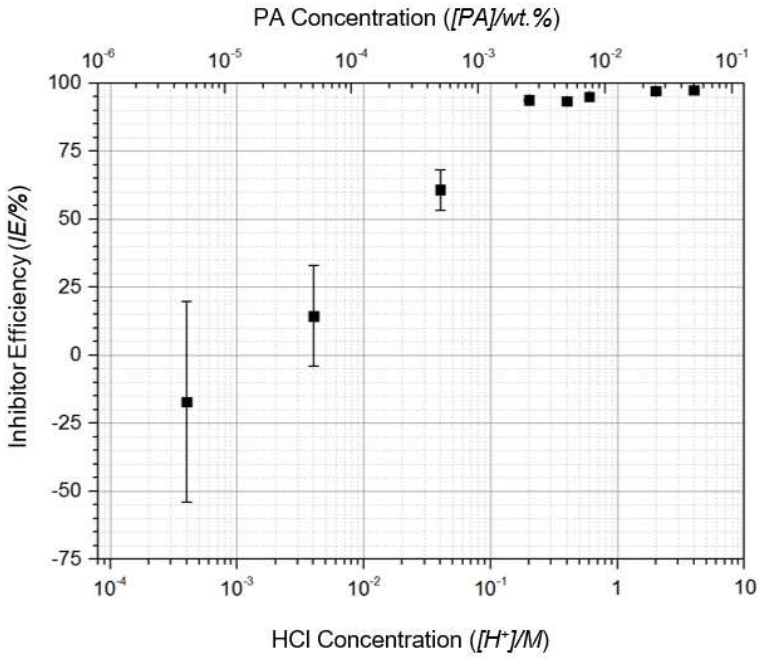

(b)

Figure 4: (a) Corrosion rates of HS80™ steel in HCl – NaCl solutions without inhibitor (3 h mass loss tests) and with propargyl alcohol (PA) (3 h mass loss and electrochemical LPR tests). Experiments were performed in static conditions in a closed 1 L vessel. HCl concentration was varied from 0.0004 to

4 M. The test solutions were prepared by diluting 4 M HCl (containing 0.05 wt.% PA) with 4 M uninhibited NaCl;
(b) Inhibitor efficiency, calculated from mass loss results, and plotted as a function of HCl concentration.
Note that a corrosion current density of 1 mA cm^{-2} is equivalent to a corrosion rate of 10.4 g m^{-2} h^{-1}, 11.6 mm $year^{-1}$ or 1.33 µm h^{-1}.

Despite the observed linear relationship between uninhibited corrosion rate and HCl concentration (Fig. 4(a)), it is important to consider the extent of acid consumption in each test. Assuming the hydrogen-evolution reaction is the only cathodic reaction in the system (i.e., neglecting oxygen and water reduction), the extent of acid consumption in each test can been calculated as shown in Table 2.

For the tests which employ a low initial HCl molarity, we observe that the calculated acid consumption approaches and *exceeds* 100%. We believe that the acid consumption data (Table 2) for the test which employs an initial HCl molarity of 0.0004 M is positively biased due to the influence of a broader range of cathodic reactions. The high extent of acid consumption in the static tests employing an initial HCl molarity ≤0.04 M will result in a significant underestimation of the corrosion rate. This effect will have an influence the relationship between uninhibited corrosion rate and initial HCl molarity (Fig. 4(a)).

A further limitation of the static tests is that the concentration of Fe^{2+} ions in the test solution increases with time, which may result in a progressive change in the surface chemistry of the test sample, as well as a change in H^+ activity observed by the steel specimens. It is particularly difficult to speculate as to the potential changes in activity throughout each static experiment, as this is influenced by both acid depletion due to reaction with the surface, but is somewhat counteracted by the increased ionic strength in the solution from the production of Fe^{2+} ions from the steel surface.

In contrast to the static tests, aside from the influence of propargyl alcohol on H^+ activity (which is likely to be minimal at the small concentration of ~0.009 M), the key effects in the flow cell can be attributed to the relative changes in HCl and NaCl molarity during the experiment, noting that the ionic strength remains constant at 4 M for the entire experiment. In essence, this simultaneous change in HCl concentration (reducing throughout the test) and NaCl concentration (increasing throughout the test) have competing effects. Reducing HCl concentration will reduce both HCl molarity and the activity coefficient of H^+, reducing the effective concentration. However, the progressive increase in NaCl content in the dilution fluid will serve to increase the activity coefficient. In terms of which effect dominates the change in activity coefficient, Jiang [24] has shown that progressive dilution of HCl with NaCl solution at 298 K results in a gradual diminution in activity coefficient from ~1.8 to 1.4 over a HCl molarity of 4 to 0.4 M, indicating that the HCl molarity dominates the

activity coefficient response. Assuming such trends extend to 80°C, this essentially means that progressive dilution results in a decline in both the molarity and activity coefficient of H^+ during the experiment.

Initial HCl Concentration (M)	Carbon steel corrosion rate from mass loss ($g\ m^{-2}\ h^{-1}$)		Inhibition Efficiency (%)	Acid consumption in static tests (%)		Equivalent Acid consumption in flow cell (10 ml min^{-1}) (%)	
	Uninhibited	Inhibited		Uninhibited	Inhibited	Uninhibited	Inhibited
4	685.6 ± 43.5	17.7 ± 0.4	97.4 ± 0.1	5.3 ± 0.3	0.3 ± 0.004	0.1	0.003
2	409.8 ± 31.2	11.8 ± 1.3	97.1 ± 0.3	6.4 ± 0.5	0.2 ± 0.02	0.1	0.004
0.6	195.7 ± 10.5	9.7 ± 0.4	95 ± 0.2	10.2 ± 0.5	0.5 ± 0.02	0.2	0.01
0.4	139.3 ± 21.2	9.3 ± 0.7	93.4 ± 0.5	10.8 ± 1.7	0.7 ± 0.06	0.2	0.01
0.2	108.2 ± 8.3	6.7 ± 0.4	93.7 ± 0.4	16.8 ± 1.3	1.1 ± 0.07	0.3	0.02
0.04	39.0 ± 1.8	15.3 ± 2.9	60.8 ± 7.5	30.4 ± 1.4	11.9 ± 2.2	0.6	0.2
$4x10^{-3}$	12.8 ± 0.9	11.0 ± 2.3	14.4 ± 18.5	99.4 ± 7.0	85.4 ± 18.2	1.9	1.6
$4x10^{-4}$	1.4 ± 0.4	1.7 ± 0.5	-17.2 ± 37.0	112.1 ± 28.0	133.1 ± 42.0	2.1	2.5

Table 2: Average corrosion rate and inhibition efficiency (given by mass loss tests) for HS80™ steel exposed to various initial HCl concentrations for 3 h at 80°C. Calculated consumption of acid expressed as a percentage of the initial HCl concentration for static tests and flow cell tests (10 ml min^{-1}).

3.2 Static mass loss tests in the inhibited HCl–NaCl solution

The influence of 0.05 wt.% PA per 1 L 4 M HCl on the corrosion rate of carbon steel is also shown in Fig. 4(a), as determined by both mass loss and electrochemical (LPR) techniques. The efficiency of the inhibitor as a function of HCl concentration is shown in Fig. 4(b), based on the mass loss measurements. It is worth noting again that the inhibitor concentration is concomitantly reduced with the acid concentration so that whilst the 4 M HCl test contains 0.05 wt% PA, the 0.0004 M HCl test contains only 0.00005 wt% PA.

Referring to Figs. 4(a) and 4(b), at the two lowest initial HCl concentrations ($4x10^{-4}$ and $4x10^{-3}$ M), the results suggest that the associated low dosages of PA have no significant effect in reducing the corrosion rate relative to uninhibited conditions. However, as discussed previously, due to acid consumption, the corrosion rate is likely to be underestimated at low initial HCl concentrations (0.04 - $4x10^{-4}$ M). This highlights limitations of the mass loss methodology when studying corrosion in dilute acids. The inhibitor performance in such low HCl concentrations was challenging to quantify.

As HCl concentration is increased along with the inhibitor dosage (Fig. 4(b)), PA efficiency improves dramatically, reaching an efficiency of ~60% in 0.04 M HCl (0.0005 wt.% or ~5 ppm PA) and >90% in 0.4 M HCl (0.005 wt.% or ~50 ppm PA). Fig. 4(a) shows that PA reduces corrosion rate from >100 g m^{-2} h^{-1} to ~10 g m^{-2} h^{-1} in 0.4 M HCl. In 4 M HCl, 0.05 wt.% or ~500 ppm PA reduces the corrosion rate from

~685 g m^{-2} h^{-1} to 18 g m^{-2} h^{-1}. This demonstrates the remarkable effectiveness of acetylenic alcohols in their ability to protect low carbon steels in concentrated acids.

3.3 Static test electrochemistry comparison with flow cell electrochemistry data and mechanism of PA inhibition in HCl–NaCl solution

Figs. 5(a) to (d) present the OCP, reciprocal of R_p and corrosion current density of the low carbon steel throughout the flow cell dilution experiment. In this experiment, 4 M HCl acid (containing 0.05 wt.% PA) is progressively diluted by 4 M NaCl at a flow rate of 10 ml min^{-1}. The temperature is maintained at 80°C. At various instances in time throughout the dilution process, the solution chemistry passing through the flow cell is identical to the initial static test chemistries shown in Table 1.

Figure 5(a) shows the OCP as a function of time for both the static tests (individual points) and repetitions of the flow cell experiment (continuous points). For comparison, OCP values from static *uninhibited* experiments (labelled 3 Hour Blank OCP) are given within this figure. Excellent repeatability is observed for the flow cell data and good agreement is seen with the OCP measured in the static tests. Figure 5(b) shows the reciprocal of R_p as a function of time. Again, good agreement is observed between the flow cell and static test data, with the exception of a lower value given by the static test at ~8 h (this test employs an initial HCl concentration of 0.04 M wherein acid consumption is appreciable based on the calculations given in Table 2).

Figs. 5(c) and 5(d) show changes in the corrosion rate determined by static mass loss tests (data converted into corrosion current densities), by static electrochemical experiments (specific Stern-Geary values were used for each test) and by duplicate flow cell experiments (assuming a Stern-Geary value of 13.3 over the entire test duration). It is perhaps inappropriate to assign a constant Stern-Geary coefficient to the entire duration of the flow cell experiment (due to the potential for the coefficient to vary with time) but this at least provides an indication of changes in the corrosion rate with time, which assists in the interpretation of PA inhibition mechanisms in the following discussion. Furthermore, the Stern-Geary coefficient extracted from the static electrochemistry experiments has a standard deviation of 1.7 (relative standard deviation ±12.7%), indicating a subtle variation with HCl molarity under inhibited conditions.

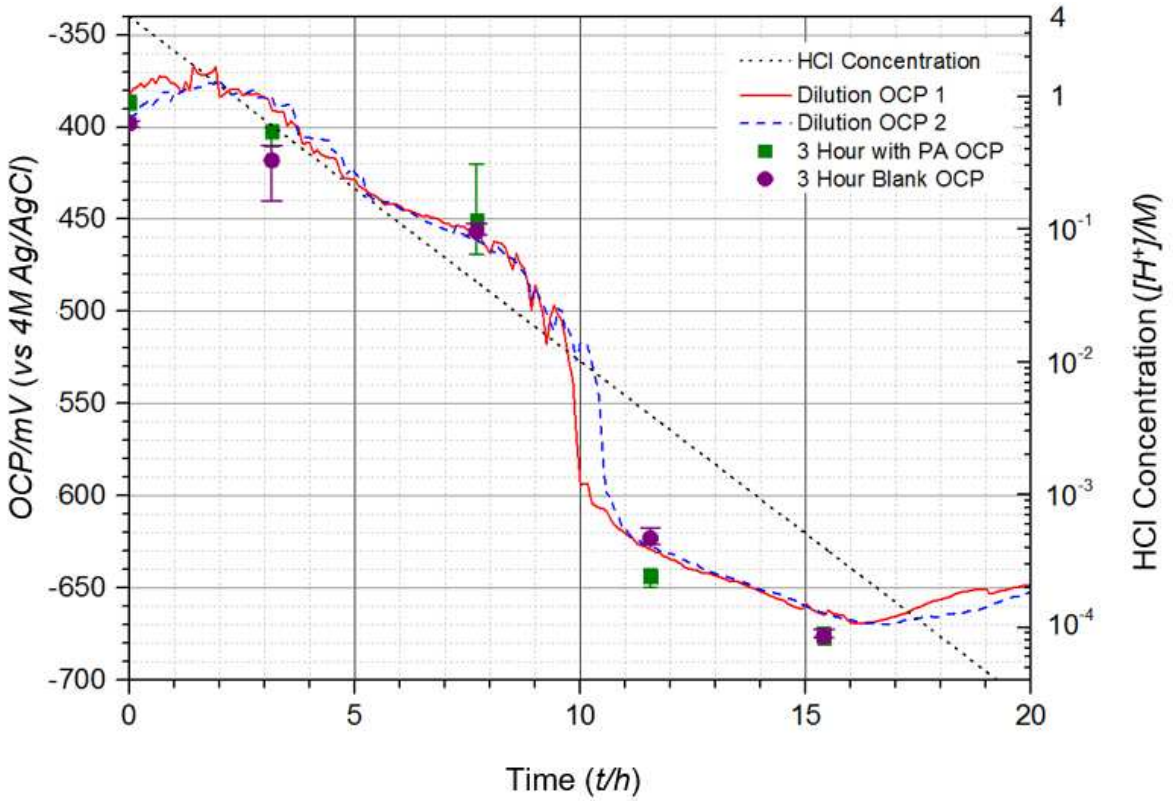
HCl Concentration
Dilution OCP 1
Dilution OCP 2
3 Hour with PA OCP
3 Hour Blank OCP
OCP/mV (vs 4M Ag/AgCl)
HCl Concentration ([H+]/M)
Time (t/h)
-350
-400
-450
-500
-550
-600
-650
-700
0
5
10
15
20
4
1
10-1
10-2
10-3
10-4

(a)

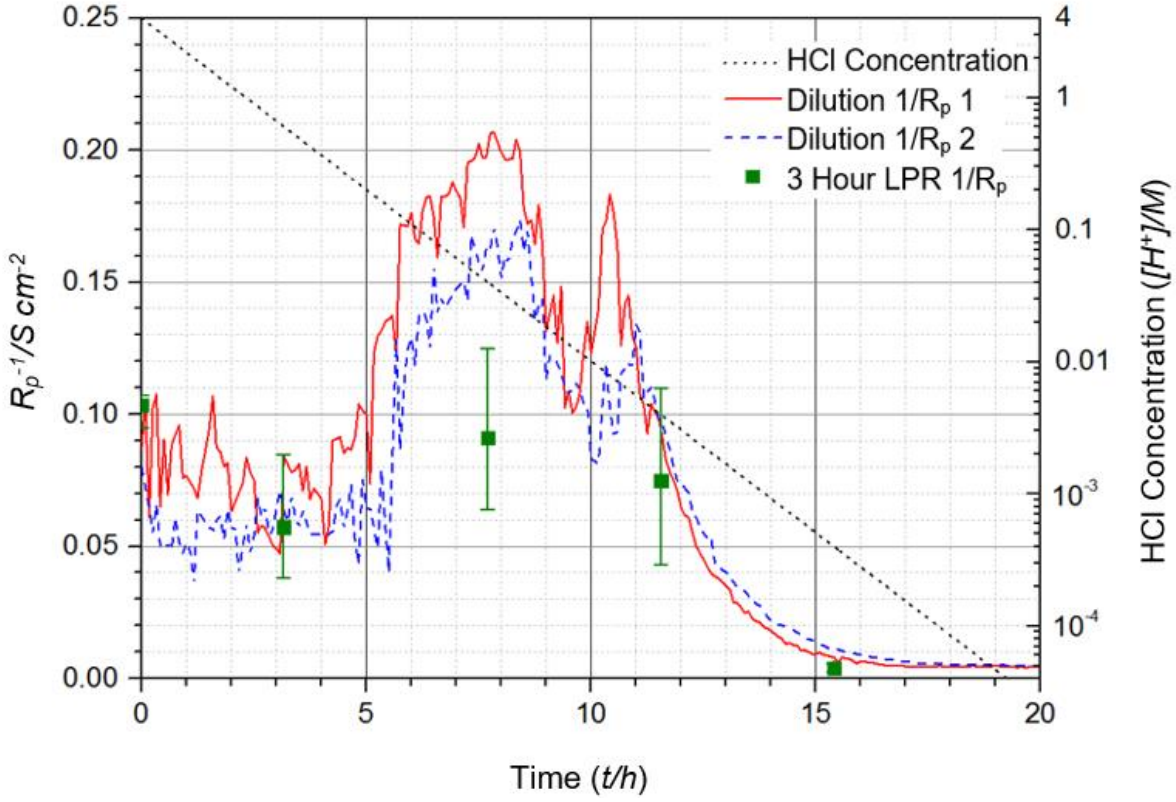
HCl Concentration
Dilution 1/Rp 1
Dilution 1/Rp 2
3 Hour LPR 1/Rp
Rp-1/S cm-2
HCl Concentration ([H+]/M)
Time (t/h)
0.25
0.20
0.15
0.10
0.05
0.00
0
5
10
15
20
4
1
0.1
0.01
10-3
10-4

(b)

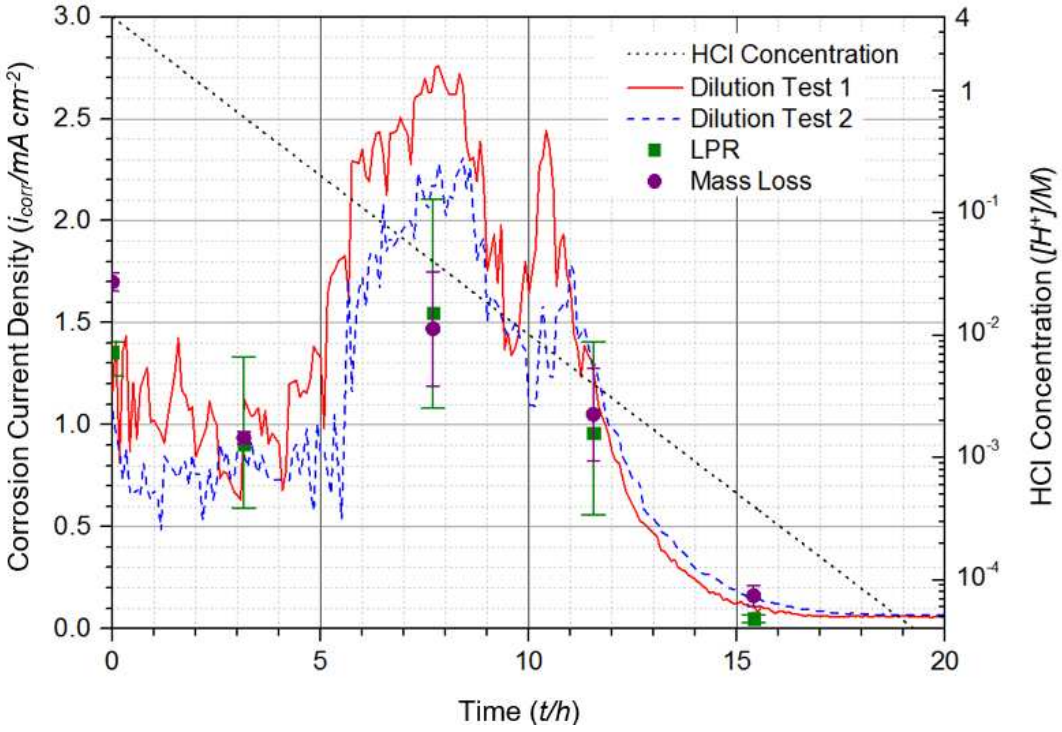

(c)

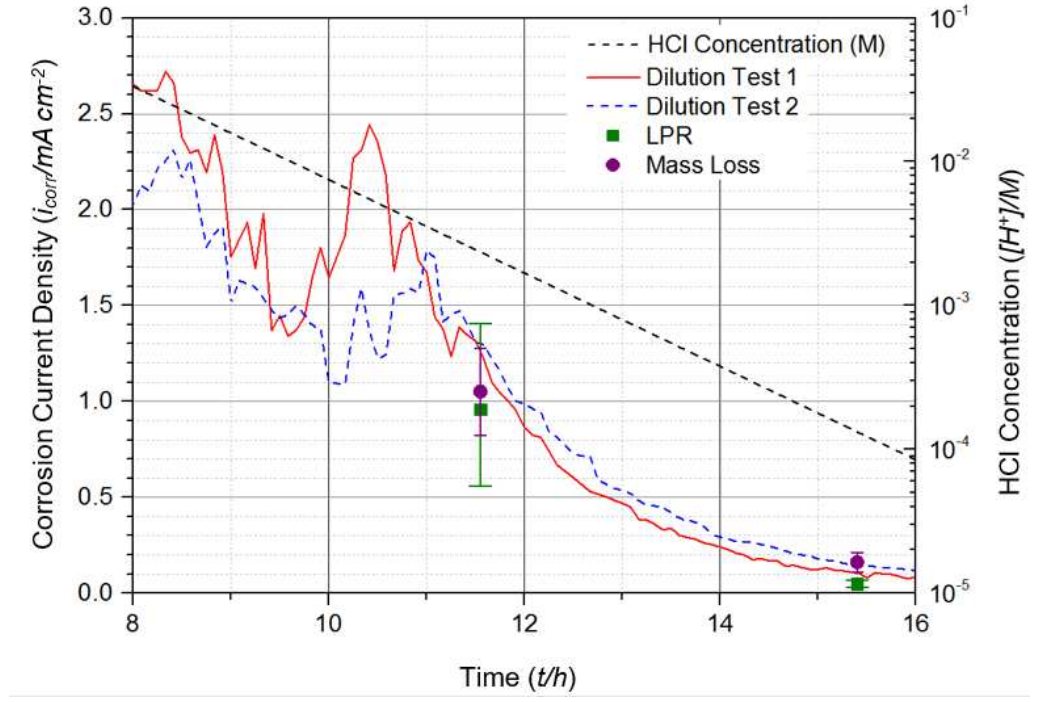

(d)

Figure 5: Comparison of (a) OCP (vs. Ag/AgCl in 4M KCl), (b) reciprocal of R_p and (c)/(d) corrosion current density in mA cm^{-2} of static 3 h experiments in a 1 L closed vessel with results determined from flow cell experiments. Individual points indicate average values from 3 h static experiments and are plotted at times corresponding to where the solution chemistry matches that flowing through the flow cell.

Before considering the data in Fig. 5 in detail, it is perhaps prudent to review what is known about the mechanism of PA inhibition. The inhibition mechanism of PA can be divided into two steps, namely, chemi-sorption of the acetylenic alcohol and its derivatives on the metal surface followed by the formation of a protective film by polymerisation on the active metal surface [8, 25-30]. The polymerisation process is surface-catalysed and promoted by acidic conditions. The polymer film developed by PA (0.2 wt. %) has been shown to form a hydrophobic film on HS80^{TM} with a thickness of 11.3±0.9 Å after immersion in 14 wt. % HCl at 78°C for 2 h. This corresponds to an equivalent thickness of almost three end-to-end monolayers of inhibitor molecules [7]. Poling [31] performed infrared studies to quantify film thickness as a function of time for polymer films formed by PA. Using a 10% HCl solution containing 87 mM (~0.47 wt%) PA, Poling reported that the polymeric inhibitor film grew to a thickness of ~60 Å after 25 h at 65°C. In addition, Poling reported that the film provided 80-90% protection when its thickness was close to that of one monolayer compared to >99% protection when the film had grown to a thickness approximating to 15 monolayers. This prior understanding of the PA inhibition process is used to decipher and explain the trends observed in the present study.

3.4 Corrosion behaviour analysis as a function of time intervals

3.4.1 Corrosion behaviour in time interval from 0 to 5 h

Referring to Figs. 5(a), 5(b) and 5(c), the initial OCP over the first 2 h of the experiment is more noble and the corrosion rate is lower than that shown by the uninhibited system (e.g., in 4 M HCl at 80ºC, -370 to -380 mV for inhibited, vs ~-400 mV for uninhibited). This indicates that the PA acts primarily as an anodic inhibitor under these conditions, agreeing with the observations of Okamoto et al. [32].

In this system, at the start of the test, the predominant electrochemical reactions at the steel surface are the dissolution of iron (ferrite) and the evolution of hydrogen. Some hydrolysis of the cementite (Fe_3C) contained within the pearlite phase is also possible due to the initial strength of the acid, as Fe_3C can be unstable under strong acid environments [33-35]. In our tests, as the solution becomes less acidic with time, the Fe_3C phase is expected to become more resistant to oxidation. As ferrite dissolution proceeds, the more stable Fe_3C phase will protrude from the steel surface creating lamellar protrusions due to the original pearlite microstructure. These protrusions provide additional surface area for the cathodic reaction. However, in time, these protrusions will be undermined by further corrosion and ultimately they will lose electrical contact with the steel surface [36]. Thus, as acid corrosion progresses, changes in the composition and surface area of the steel surface will influence corrosion rate. Protrusions of Fe_3C will tend to promote galvanic corrosion.

Good agreement between the flow cell data and data given by the individual static electrochemical experiments is observed for the first 5 h of the experiment as shown

in Figure 5. The stable corrosion rate observed during this period suggests that PA is able to maintain film integrity on the steel surface.

3.4.2 Corrosion behaviour in time interval from 5 to 8 h

After 5±0.5 h, the corrosion rate rises sharply and continues to rise during the period until 8 h. Over this period, we observe a gradual decline in the OCP, during which, both the molarity of H^+ and the concentration of PA are decreasing with time. Such a decrease in H^+ concentration would be expected to yield a decrease in the OCP for an *uninhibited* system based on the Nernst relationship for the cell potential and a decrease in the rate of the cathodic reaction. Even though the H^+ concentration is decreasing during the period 5 to 8 h, the corrosion rate is *increasing*. This must be due to significant loss in the integrity of the polymeric film resulting in an increase in the rate of the anodic reaction. It should be noted that whilst we observe a significant increase in corrosion rate during the period 5 to 8 h, all the corrosion rates measured during this period are well below uninhibited corrosion rates for the equivalent HCl molarity range. This indicates only a *partial* degradation of the polymeric film.

We suggest that the initial rise in corrosion rate at 5±0.5 h is triggered by the concentration of PA falling below some critical limit below which the polymeric film cannot be maintained or rehealed. This suggestion is consistent with observations reported by Barmatov et al. [37], Growcock and Lopp [26] and Frenier et al. [29]. Barmatov et al.[37] demonstrated that insufficient inhibitor in the bulk solution can play a major role in the mechanism of degradation of a polymerisable inhibitor film. Both Growcock and Lopp [26] and Frenier et al. [29] proposed that for long-term protection, the concentration of inhibitor in the bulk solution should be maintained above a critical level.

At the 8 h mark, the reciprocal of R_p (Fig. 5(b)) and the corrosion current density (Fig. 5(c)) pass through a maximum that defines the first of two peaks as the dilution process proceeds to 20 h. At this first peak, there exists the greatest discrepancy between the flow cell response and the static electrochemistry/mass loss data. This is likely to be related to the difference in the condition of the steel surface at this point as compared to that in the static experiments. Other key differences are the effect of dynamic flow conditions on a partially degraded polymeric film and the effect of acid consumption in the static experiments. It is known that the surface conditions generated during a pre-corrosion period have an important influence on the corrosion rate and inhibition efficiency. Barmatov et al. [33] showed that PA is less efficient on precorroded steel surfaces compared to freshly ground specimens (in 4 M HCl, 0.05wt% PA is 10-15% less efficient on the precorroded surface as compared to the freshly ground surface).

At 8 h, the HCl concentration moving through the flow cell is 0.04 M. In separate 3 h static tests, we determined the *uninhibited* corrosion rate in 0.04 M HCl to be ~38.6 g m^{-2} h^{-1}; this is likely to be an underestimate due to significant acid consumption. By

comparison, the corrosion rate at 8 h (0.04 M HCl + 0.0005 wt.% PA) in the flow cell is 22-27 g m^{-2} h^{-1} and 11-22 g m^{-2} h^{-1} from equivalent static experiments which suggests that some residual inhibition is provided by the film. Thus, we conclude that the first peak at 8 h is not given by full desorption of the inhibitor film, merely by a reduction in the protectiveness of the film.

3.4.3 Corrosion behaviour in time interval from 10 to 20 h

Beyond the first peak at 8 h, we observe that the corrosion rate and OCP sharply decrease but then, after 10±0.5 h, the corrosion rate increases again accompanied by a sharp decrease in OCP. Again, we attribute the increase in corrosion rate during the interval 10–11 h to an acceleration of the rate of the anodic reaction. This period is marked by a sharp change in OCP, specifically a cathodic shift of 100 mV in less than 1 h. We suggest that during this period there is significant degradation and desorption of the film resulting in corrosion rates which are similar to uninhibited rates under equivalent acid conditions. Beyond the second peak at 11 h, the corrosion rate gradually decreases until a steady state is reached beyond 16 h. This steady state corrosion rate is ~0.7 g m^{-2} h^{-1}, which is indicative of the 4 M NaCl solution.

To further understand the inhibition behaviour of PA beyond the second peak, a set of constant composition experiments were performed using the flow cell. A HCl molarity of 0.05 M was chosen because this is the HCl concentration just beyond the second peak observed during the flow cell dilution experiment. Uninhibited 0.05 M HCl was fed through the flow cell for 2 h before the solution was switched to 0.05 M HCl containing either 0.01 or 0.25 wt.% PA. The results are shown in Fig. 6 and indicate that 0.01 or 0.25 wt.% PA has no noticeable effect on the corrosion rate of HS80™ under these conditions. Consequently, we can conclude that the second peak observed in the flow cell dilution experiment is given by complete film degradation and desorption of PA.

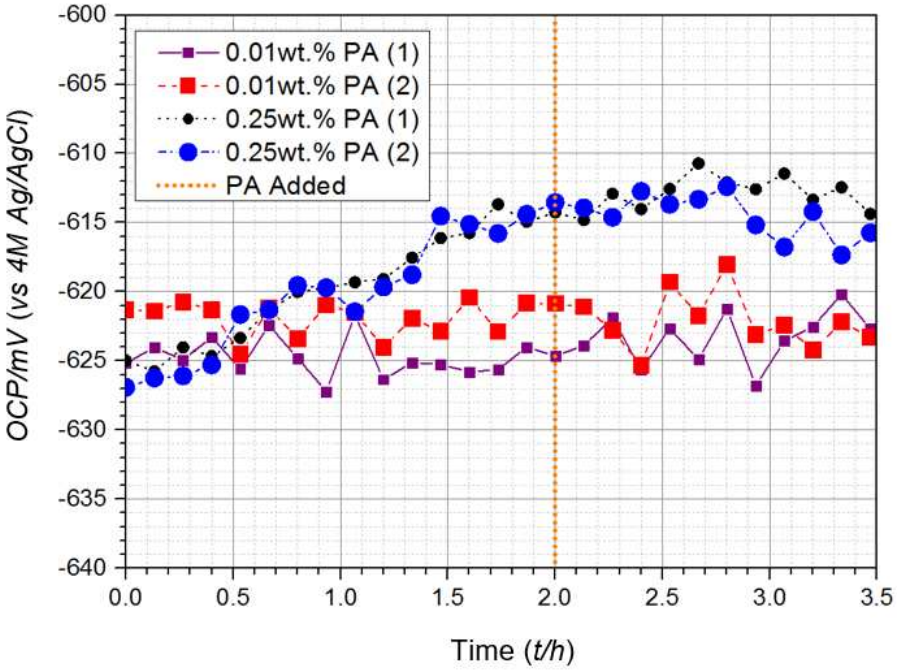

(a)

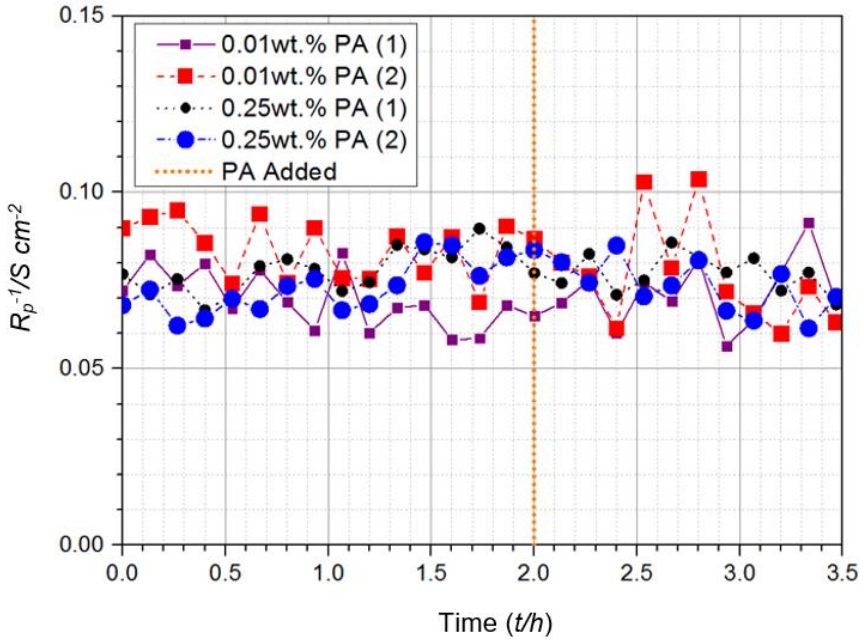

(b)

Figure 6: (a) OCP (vs. Ag/AgCl in 4M KCl) and (b) the reciprocal of R_p as a function of time for constant composition experiments using the once-through flow cell. Uninhibited 0.05 M HCl containing 3.95 M NaCl is pumped through the cell at 10 ml min^{-1} before the addition of either 0.01 or 0.25 wt.% PA (per litre of 4 M HCl used to formulate the HCl-NaCl solution).

3.5 Effect of flow/dilution rate and inhibitor concentration on the corrosion performance of PA during transitions in fluid composition

As mentioned previously, in the field application, the duration of the acid flowback period is predominantly governed by the quantity of unreacted acid remaining in the

near-wellbore region and the production rate. The following sections focus on the effects of flowback rate (or rate of HCl dilution) and the effects of inhibitor concentration to gain a better understanding of the sensitivity of the system to key operating parameters and to enhance our understanding of the PA inhibition mechanisms.

3.5.1 Effect of flow/dilution rate

Three flow rates of 5, 10 and 15 ml min^{-1} were used in further flow cell dilution experiments. For each flow rate, changes in the HCl concentration with time are given in Fig. 3.

For each flow rate, the initial acid and PA concentrations were kept constant at 4 M and 0.05 wt.%, respectively. For each flow rate, the reciprocal of R_p and the OCP data are plotted as a function of time and HCl concentration in Figs. 7(a)–7(d).

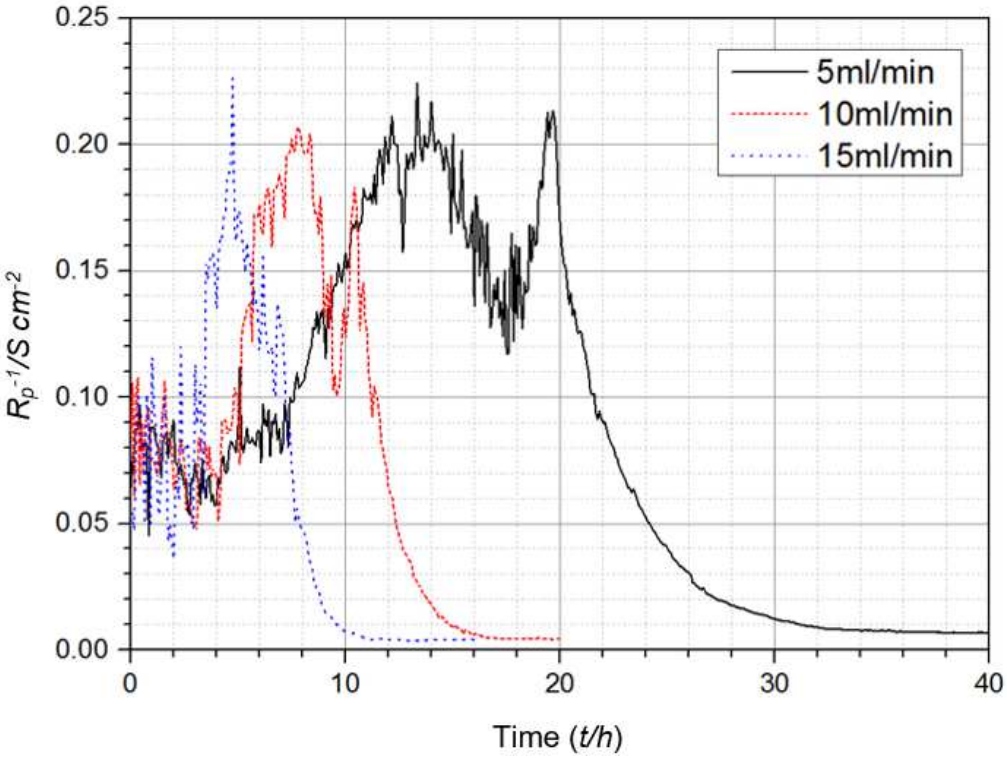

(a)

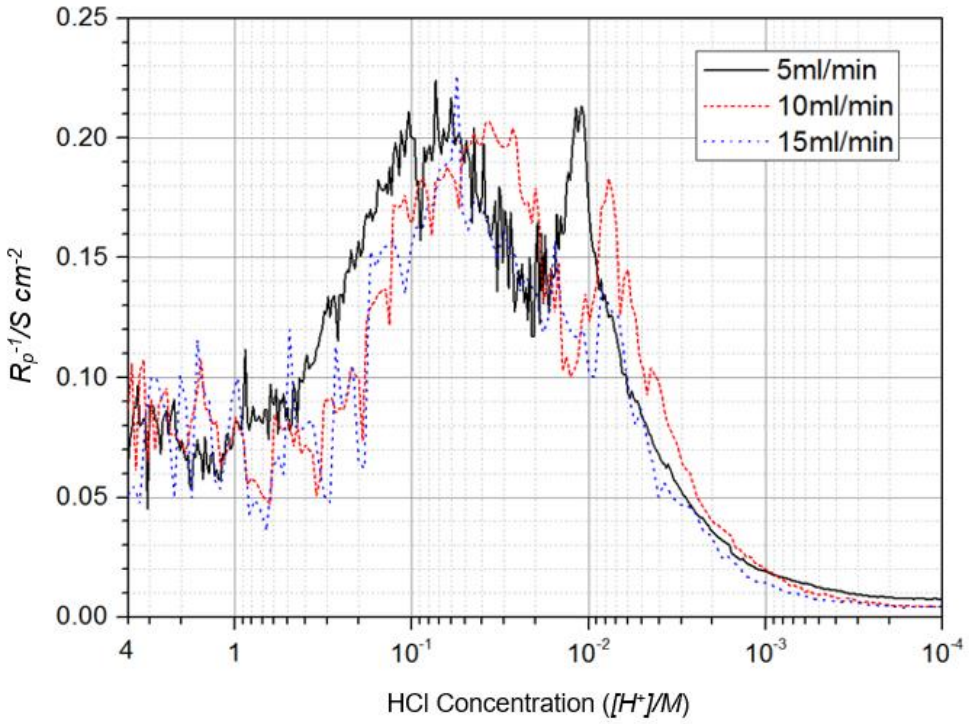
0.25
0.20
0.15
0.10
0.05
0.00
R_p^{-1}/S cm^{-2}
5ml/min
10ml/min
15ml/min
4
1
10^{-1}
10^{-2}
10^{-3}
10^{-4}
HCl Concentration ([H^+]/M)

(b)

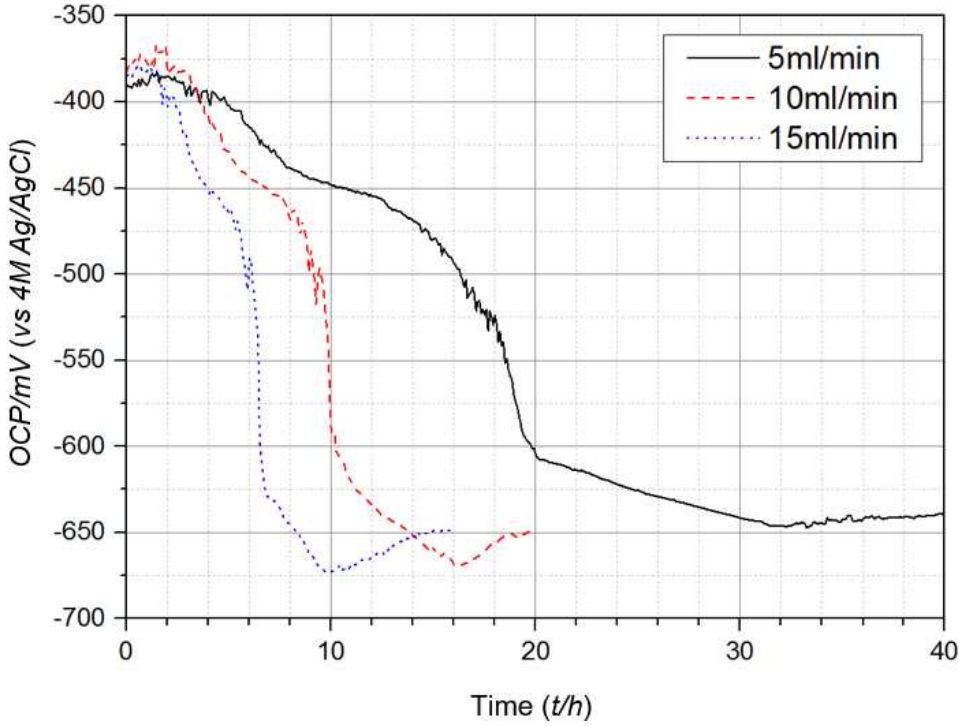
-350
-400
-450
-500
-550
-600
-650
-700
OCP/mV (vs 4M Ag/AgCl)
5ml/min
10ml/min
15ml/min
0
10
20
30
40
Time (t/h)

(c)

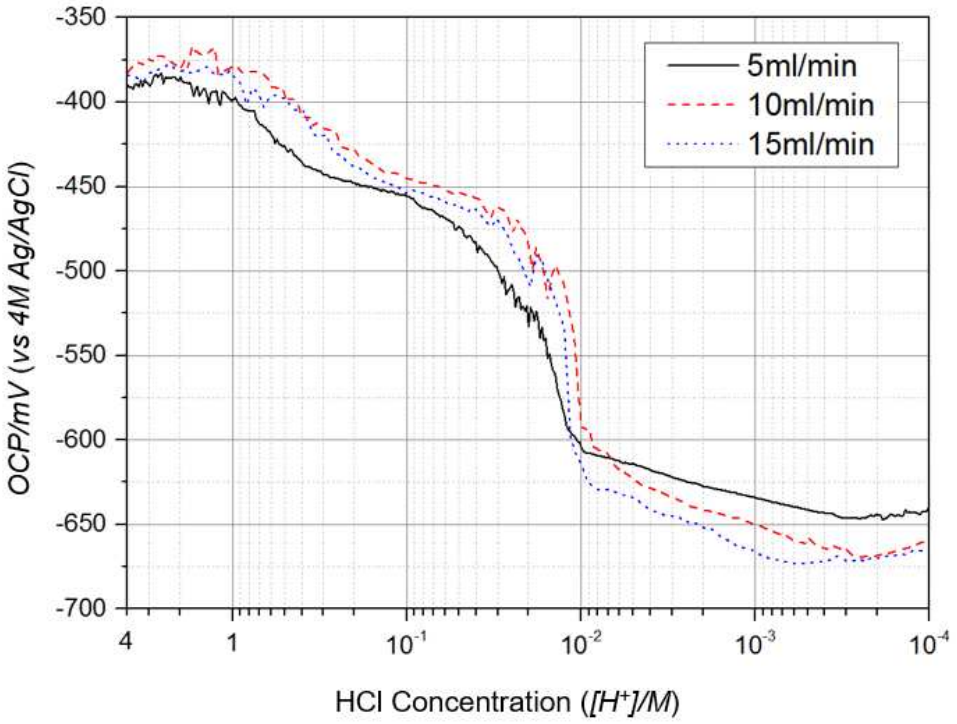

(d)

Figure 7: Comparison of (a)/(b) reciprocal of R_p and (c)/(d) OCP (vs. Ag/AgCl in 4M KCl) during the course of three flow cell tests performed at different flow rates (5, 10 and 15 ml min^{-1}) at 80ºC. In these experiments, 4 M HCl (containing 0.05 wt.% PA) was diluted with 4 M uninhibited NaCl solution and pumped through the flow cell at 5, 10, or 15 ml min^{-1}. Graphs (a) and (c) show the variation in 1/R_p and OCP as a function of time, and graphs (b) and (d) show the same data plotted as a function of HCl concentration within the flow cell at the time of measurement.

By plotting the reciprocal of R_p and the OCP as a function of the HCl concentration within the flow cell, a direct comparison can be made between the dilution tests performed using the three different flow rates. The data shown in Fig. 7(b) suggest that, for a given HCl concentration in the flow cell, the evolution of the R_p reciprocal does not vary significantly. Similar maximum values for the reciprocal of R_p (0.2~0.23 S·cm^2) are recorded when the HCl concentration in the flow cell lies in the range 0.04–0.07 M. We note that there are significant differences in the magnitude of the second peak when different flow rates are employed; a smaller second peak is observed for the experiment performed at 15 ml min^{-1}. The OCP data plotted in Fig. 7(d) confirm that the onset of the second peak is highly correlated to a sharp cathodic shift.

3.5.2 Effect of inhibitor concentration

Fig. 8 compares the results of three flow cell dilution experiments, each performed at a flow rate of 10 ml min^{-1}, but using three different PA concentrations in the initial 4 M HCl solution. Fig. 8(a) shows that increasing the initial PA concentration reduces the *average* corrosion rate over the entire duration of the test. The initial PA concentration influences the position and magnitude of the first peak and the magnitude of the second peak. The onset of the first peak is increasingly delayed as the initial PA concentration increases. This onset occurs after 2 h for an initial PA concentration of 0.01 wt.% and after ~8 h for an initial concentration of 0.25 wt.%. In contrast, the initial PA concentration does not affect the onset of the second peak, which occurs after ~10 h in each case. There is no effect of the initial PA concentration on the OCP during the period 8 to 18 h and, again, we observe, a sharp cathodic shift at the onset of the second peak.

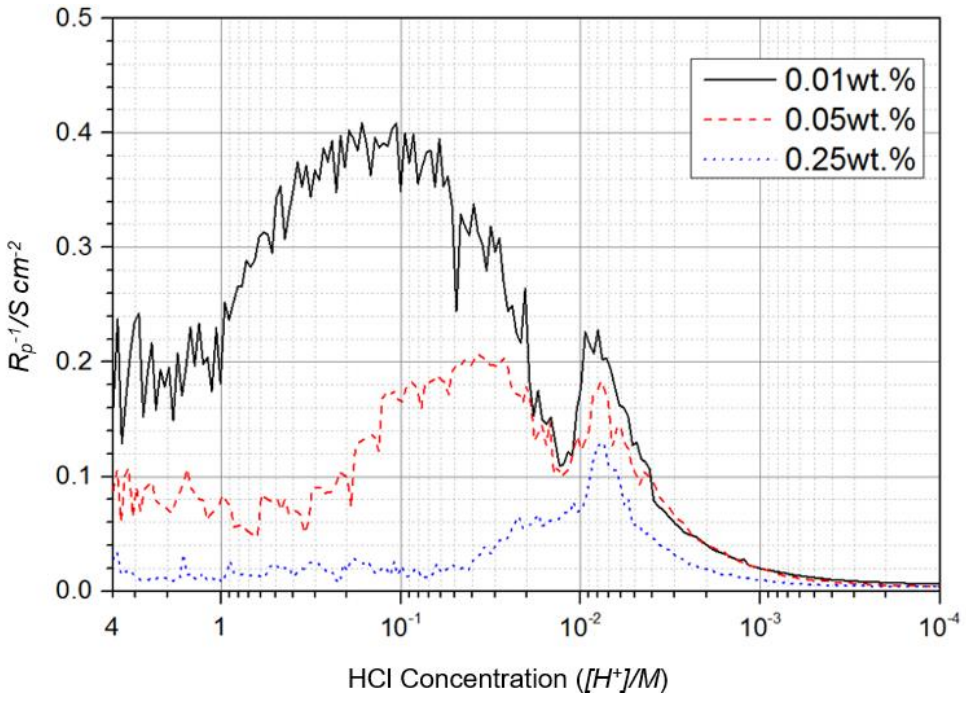

(a)

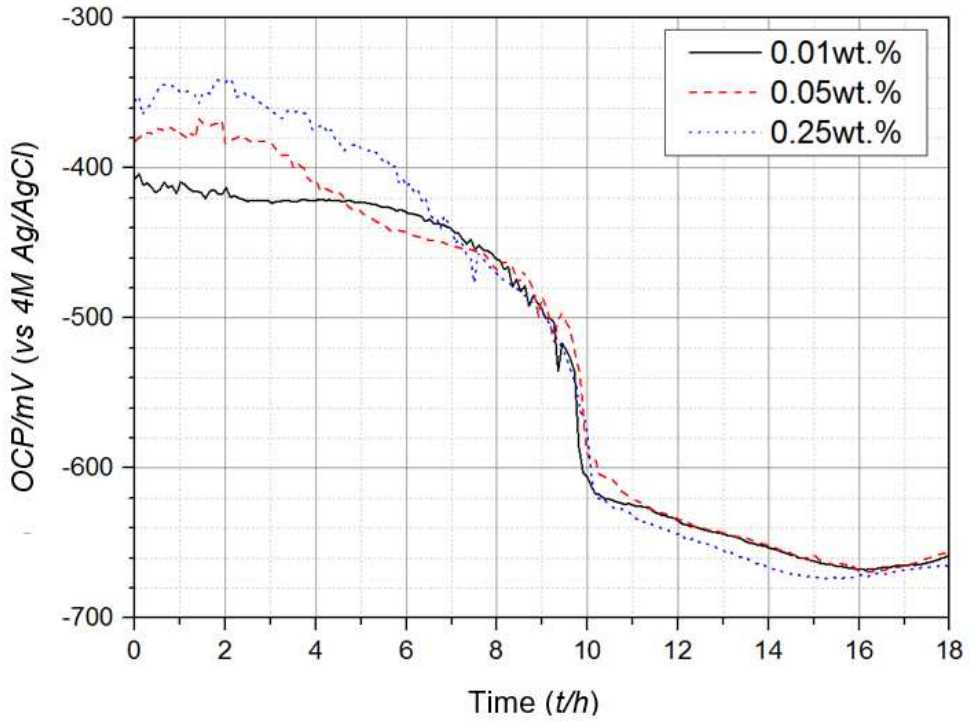

(b)

Figure 8: Comparison of (a) reciprocal of R_p and (b) OCP (vs. Ag/AgCl in 4M KCl) during the course of three flow cell tests performed with different initial PA concentrations (0.01, 0.05 and 0.25 wt.% in 4 M HCl) at 80°C.

3.5.3 Observations regarding *critical* concentrations of HCl and PA

Fig. 9 compares plots of the R_p reciprocal as a function of the HCl concentration (Fig. 9(a)) and as a function of the PA concentration (Fig.9(b)) in the flow cell.

Fig. 9(a) shows that, as the initial PA concentration increases, the first peak is delayed to a position when a lower HCl concentration is passing through the flow cell. This position occurs at ~1 M HCl for an initial PA concentration of 0.01 wt.% and at ~0.04 M HCl for an initial PA concentration of 0.25 wt.%. In contrast, the second peak occurs when the HCl concentration passing through the cell is ~8×10^{-3} M, regardless of the initial PA concentration.

Fig. 9(b) shows that the position of the first peak is controlled by a critical concentration of PA. The onset of the first peak occurs at a position when the PA concentration in the cell is in the range $2\text{x}10^{-3}$ to $3\text{x}10^{-3}$ wt.%, regardless of the initial PA concentration. In contrast, when plotted as a function of PA concentration in the cell, the position of the second peak varies with the initial PA concentration.

In summary, when the initial PA concentration is varied in the range 0.01–0.25 wt.%, the first peak occurs at different HCl concentrations passing through the cell (Fig. 9(a)) but at a very similar PA concentration ($2\text{x}10^{-3}$ to $3\text{x}10^{-3}$ wt.%). In contrast, the same experiments revealed that the position of the second peak is controlled by a

critical HCl concentration passing through the cell, viz. ~8×10^{-3} M, regardless of the initial PA concentration.

Thus, the onset and position of the first peak are controlled by a critical concentration of PA rather than a critical concentration of HCl. As discussed previously, this observation is consistent with the idea that a critical concentration of PA is required to maintain (or reheal) the polymeric film. When the PA concentration in the cell falls below this critical concentration, the polymeric film partially degrades leading to an increase in corrosion rate (the first peak). Again, this is consistent with findings reported by Barmatov et al. [37], Growcock and Lopp [26] and Frenier et al. [29].

The onset and position of the second peak are controlled by a critical concentration of HCl. Our data suggest that there is a critical HCl concentration below which the polymeric film cannot be maintained and it, therefore, degrades. This is consistent with the observations of Aramaki and Fujioka [8] who demonstrated that PA functions best in low pH solutions (noting that PA requires H^+ ions to catalyse its intermediate reaction). In addition, Poling [31] suggested that hydrogen evolved by the acid corrosion reaction was necessary for the polymerisation of acetylenic alcohols.

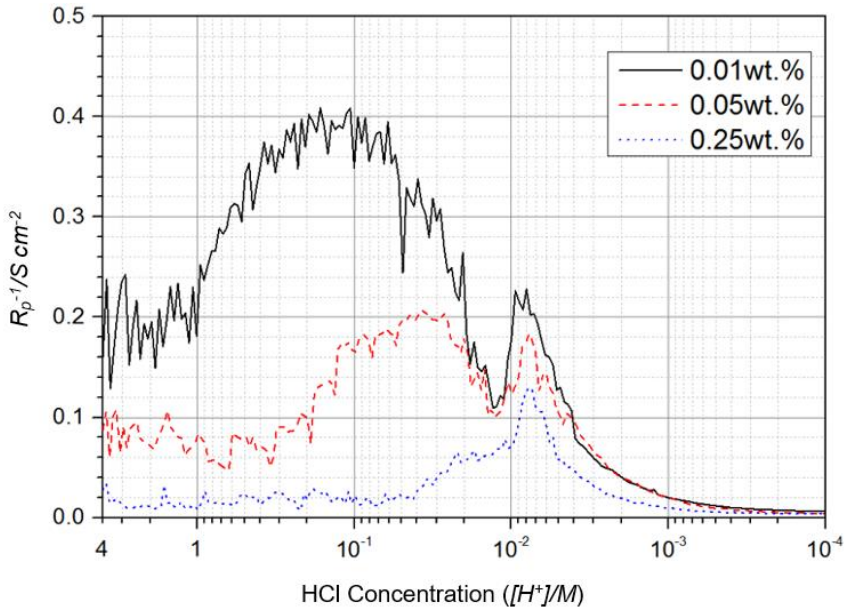

(a)

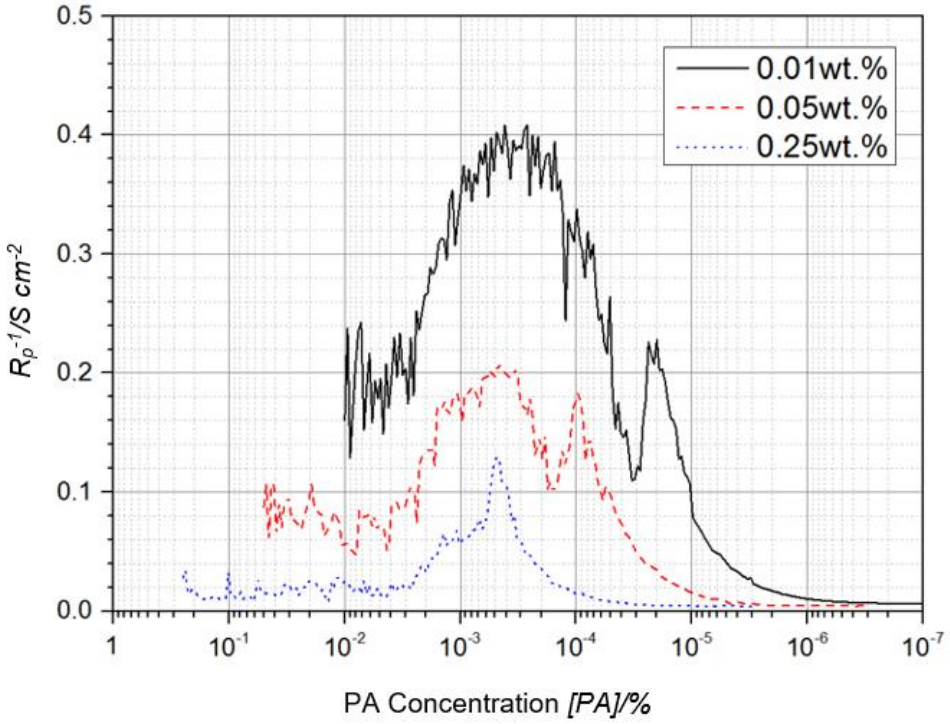

(b)

Figure 9: Comparison of the reciprocal of R_p during the three flow cell tests performed with different initial PA concentrations (0.01, 0.05 and 0.25 wt.% in 4 M HCl). Values of $1/R_p$ are plotted as a function of (a) the corresponding HCl concentration and (b) the corresponding PA concentration passing through the flow cell at the time of measurement.

4. Conclusions

A newly developed flow cell technique was applied to determine the progressive corrosion behaviour of carbon steel exposed to a fluid transition from hydrochloric acid (4 M) containing the polymerisable inhibitor propargyl alcohol (PA) to a sodium chloride solution (4 M) without inhibitor. Several fluid transition experiments each performed under isothermal conditions (80°C) were used to interpret the complex corrosion behaviour observed in the flow cell. These studies have led to an enhanced understanding of (i) PA inhibition mechanisms and (ii) progressive corrosion behaviour during matrix acidizing flowback operations.

The fluid transition experiments involve initial exposure of the carbon steel to 4 M HCl containing 0.01, 0.05 or 0.25 wt.% PA inhibitor followed by exposure to decreasing acid and inhibitor concentrations due to a progressive controlled dilution with 4 M sodium chloride. In all the experiments, we observe a sequence of different corrosion behaviour. In the first phase, the inhibited acid creates an inhibitor film which provides a high inhibition efficiency for several hours until the PA concentration flowing through the cell decreases below a critical level, viz. ~0.002–0.003 wt. %. Beyond this point, the corrosion rate rises due to a *partial* loss of film integrity and, subsequently, the corrosion rate reaches a maximum that defines a

first peak in the profiles. Subsequently, after further dilution, we observe a second peak in the corrosion rate profiles. The onset and position of the second peak are controlled by a critical concentration of HCl. Our data suggest that there is a critical HCl concentration below which the polymeric film cannot be maintained and it, therefore, completely degrades. Indeed, further constant composition flow cell tests confirmed that PA is not an effective inhibitor when used in *dilute* HCl solutions such as 0.05 M HCl; rather, PA is activated and highly efficient in stronger acid solutions.

Through comparison with static mass loss test methodologies, it can be concluded that the flow cell can more reliably determine corrosion behaviour in the dilute acid regime generated by displacing 4 M HCl containing inhibitor (simulating the unspent acid) by 4 M NaCl solution (simulating the formation brine). In future, the progressive corrosion behaviour of other representative steel substrates during the displacement of more complex unspent acid formulations by more realistic formation brine chemistries could be studied using the flow cell approach. This would enhance our knowledge of the complex corrosion behaviour encountered during the acid flowback process.

5. Acknowledgements

The authors would like to thank EPSRC and Schlumberger Cambridge Research for providing the funding which made this research possible.

6. Data Availability

The raw/processed data required to reproduce these findings cannot be shared at this time as the data also forms part of an ongoing study.

7. References

[1] R. Barker, B. Pickles, N. Kapur, T. Hughes, E. Barmatov, A. Neville, Flow cell apparatus for quantitative evaluation of carbon steel corrosion during transitions in fluid composition: Application to transition from inhibited hydrochloric acid to sodium chloride brine, Corrosion Science, (2018).

[2] B.B. Williams, J.L. Gidley, R.S. Schechter, Acidizing Fundamentals, Henry L. Doherty Memorial Fund of AIME, Society of Petroleum Engineers of AIME, 1979.

[3] M.J. Economides, K.G. Nolte, Reservoir Stimulation, Wiley, Chichester, England; New York, 2000.

[4] S.A. Ali, L. Kalfayan, C.T. Montgomery, Acidizing, SPE, 2016.

[5] S. Al-Harthy, Oscar Bustos, Matthew Samuel, John Still, Michael J. Fuller, Nurul Ezalina Hamzah, Mohd Isal Pudin bin Ismail, A. Parajat, Options for high temperature well stimulation, Oilfield Review, 20 (2008).

[6] M. Finšgar, J. Jackson, Application of corrosion inhibitors for steels in acidic media for the oil and gas industry: A review, Corrosion Science, 86 (2014) 17-41.

[7] E. Barmatov, J. Geddes, T. Hughes, M. Nagl, Research On Corrosion Inhibitors For Acid Stimulation, in: Corrosion, NACE International, Salt Lake City, UT, 2012.

[8] K. Aramaki, E. Fujioka, Spectroscopic Investigations on the Inhibition Mechanism of Propargyl Alcohol for Iron Corrosion in Hydrochloric Acid at Elevated Temperatures, CORROSION, 53 (1997) 319-326.

[9] A. Hayatdavoudi, A. Ghalambor, V. Veludandi, Application of a New Technique in Acid Flowback Analysis, in: SPE Formation Damage Control Symposium, Society of Petroleum Engineers, Lafayette, Louisiana, 1996.

[10] L.N. Morgenthaler, P.R. Rhodes, L.L. Wheaton, Testing the Corrosivity of Spent HCl/HF Acid to 22 Cr and 13 Cr Stainless Steels, in: International Symposium on Oilfield Chemistry, Society of Petroleum Engineers, Houston, Texas, 1997.

[11] K.C. Taylor, H.A. Nasr-El-Din, Flowback Analysis of Acid Stimulation of Seawater Injection Wells: Case Histories, in: SPE International Symposium on Formation Damage Control, Society of Petroleum Engineers, Lafayette, Louisiana, 2000.

[12] M.K. Hashem, H.A. Nasr-El-Din, J.A. Hopkins, An Experience in Acidizing Sandstone Reservoirs: A Scientific Approach, in: SPE Annual Technical Conference and Exhibition, Society of Petroleum Engineers, Houston, Texas, 1999.

[13] ASTM, Standard Practice for Laboratory Immersion Corrosion Testing of Metals, in: ASTM G31-72, ASTM International, West Conshohocken, Pennsylvania, 2004.

[14] E. Barmatov, T. Hughes, M. Nagl, Performance of Organic Corrosion Inhibitors on Carbon Steels and High Alloys in 4M Hydrochloric Acid, in: CORROSION, NACE International, Dallas, Texas, 2015.

[15] E. Barmatov, T. Hughes, D. Eskin, Effect of surface roughness on corrosion behaviour of low carbon steel in inhibited 4 M hydrochloric acid under laminar and turbulent flow conditions, Corrosion Science, 103 (2015) 196-205.

[16] M.A. Quaraishi, M.Z.A. Rafiquee, N. Saxena, S. Khan, Inhibition of mild steel corrosion in presence of fatty acid imidazolines in hydrochloric acid, Protection of Metals, 44 (2008) 91-98.

[17] A.K. Singh, M.A. Quraishi, Effect of Cefazolin on the corrosion of mild steel in HCl solution, Corrosion Science, 52 (2010) 152-160.

[18] C.F. Smith, F.E. Dollarhide, N.J. Byth, Acid Corrosion Inhibitors - Are We Getting What We Need?, SPE-5644-PA, 30 (1978).

[19] W.E. Billings, D. Morris, Effect of Acid Volume and Inhibitor Quantity On Corrosion of Steel Oil Field Tubing in Hydrochloric Acid, CORROSION, 17 (1961) 208-214.

[20] W.W. Frenier, Hill, D.G. and Jasinski, R, Corrosion inhibitors for acid jobs, Oilfield Review, 1 (1989).

[21] R.L. Wabeke, Air contaminants and industrial hygiene ventilation: A handbook of practical calculations, problems, and solutions, CRC Press, 1998.

[22] P.B. Mathur, T. Vasudevan, Reaction Rate Studies for the Corrosion of Metals in Acids—I, Iron in Mineral Acids, CORROSION, 38 (1982) 171-178.

[23] A.A. Khadom, Aprael S. Yaro, Abdul Amir H Kadum, Ahmed S. Altaie, A.Y. Musa, The effect of temperature and acid concentration on corrosion of low carbon steel in hydrochloric acid media, American Journal of Applied Sciences, 6 (2009) 1403-1409.

[24] C. Jiang, Activity Coefficients of Hydrochloric Acid in Concentrated Electrolyte Solutions. 1. HCl+NaCl+H_2O, HCl+LiCl+H_2O, and HCl+$BaCl_2$+H_2O at 298.15 K, Journal of Chemical & Engineering Data, 41 (1996) 113-116.

[25] N.I. Podobaev, Y.G. Avdeev, A Review of Acetylene Compounds as Inhibitors of Acid Corrosion of Iron, Protection of Metals, 40 (2004) 7-13.

[26] F.B. Growcock, V.R. Lopp, The inhibition of steel corrosion in hydrochloric acid with 3-phenyl-2-propyn-1-ol, Corrosion Science, 28 (1988) 397-410.

[27] F.B. Growcock, V.R. Lopp, R.J. Jasinski, Corrosion Protection of Oilfield Steel with 1-Phenyl-2-Propyn-1-Ol, Journal of The Electrochemical Society, 135 (1988) 823-827.

[28] V. Farafonov, M. Grovu, C. Simionescu, Electrochemical polymerization of acetylenic derivatives. I. Anionic polymerization of phenylacetylene and diphenyldiacetylene, Journal of Polymer Science: Polymer Chemistry Edition, 15 (1977) 2041-2042.

[29] W.W. Frenier, F.B. Growcock, V.R. Lopp, Mechanisms of Corrosion Inhibitors Used in Acidizing Wells, SPE Production Engineering, 3 (1988) 584-590.

[30] Y.G. Avdeev, N.I. Podobaev, The Role of Acrolein in the Inhibition of the Acid Corrosion of Iron with Propargyl Alcohol, Protection of Metals, 41 (2005) 592-596.

[31] G. Poling, Infrared studies of protective films formed by acetylenic corrosion inhibitors, Journal of The Electrochemical Society, 114 (1967) 1209-1214.

[32] G. Okamoto, M. Nagayama, J. Kato, T. Baba, Effect of organic inhibitors on the polarization characteristics of mild steel in acid solution, Corrosion Science, 2 (1962) 21-27.

[33] E. Barmatov, T.L. Hughes, Effect of corrosion products and turbulent flow on inhibition efficiency of propargyl alcohol on AISI 1018 mild carbon steel in 4M hydrochloric acid, Corrosion Science, 123 (2017) 170-181.

[34] L.J.E. Hofer, Nature of the carbides of iron, U. S. Dept. of the Interior, Bureau of Mines, Washington, 1966.

[35] T.Y. Kosolapova, Carbides: Properties, Production, and Applications, Plenum Press, New York-London, 1971.

[36] R. Nyborg, E. Gulbrandsen, T. Loeland, K. Nisancioglu, Effect of steel microstructure and composition on inhibition of CO2 corrosion, in: CORROSION 2000, NACE International, 2000.

[37] E. Barmatov, T. Hughes, M. Nagl, Efficiency of film-forming corrosion inhibitors in strong hydrochloric acid under laminar and turbulent flow conditions, Corrosion Science, 92 (2015) 85-94.